applied sciences

MDPI

Article

Comparison of Approaches for Data Analysis of Multi-Parametric Monitoring Systems: Insights from the Acuto Test-Site (Central Italy)

Matteo Fiorucci *, Salvatore Martino, Francesca Bozzano and Alberto Prestininzi

Earth Sciences Department of "Sapienza" University of Rome and CERI-Research Centre for Geological Risk, P.le Aldo Moro n.5, I-00185 Rome, Italy; salvatore.martino@uniroma1.it (S.M.); francesca.bozzano@uniroma1.it (F.B.); alberto.prestininzi@uniroma1.it (A.P.)

* Correspondence: matteo.fiorucci@uniroma1.it; Tel.: +39-06-4991-4835

Received: 1 October 2020; Accepted: 20 October 2020; Published: 29 October 2020

Abstract: This paper deals with monitoring systems to manage the risk due to fast slope failures that involve rock masses, in which important elements (such as infrastructures or cultural heritages, among the others) are exposed. Three different approaches for data analysis were here compared to evaluate their suitability for detecting mutual relations among destabilising factors, acting on different time windows, and induced strain effects on rock masses: (i) an observation-based approach (OBA), (ii) a statistics-based approach (SBA) and (iii) a semi-empirical approach (SEA). For these purposes, a test-site has been realised in an abandoned quarry in Central Italy by installing a multi-parametric monitoring sensor network on a rock wall able to record strain effects induced by natural and anthropic forcing actions (like as temperature, rainfall, wind and anthropic vibrations). The comparison points out that the considered approaches allow one to identify forcing actions, responsible for the strain effects on the rock mass over several time windows, regarding a specific size (i.e., rock block dimensional scale). The OBA was more suitable for computing the relations over short- to medium time windows, as well as the role of impulsive actions (i.e., hourly to seasonal and/or instantaneous). The SBA was suitable for computing the relations over medium- to long time windows (i.e., daily to seasonal), also returning the time lag between forcing actions and induced strains using the cross-correlation statistical function. Last, the SEA was highly suitable for detecting irreversible strain effects over long- to very long-time windows (i.e., plurennial).

Keywords: multi-parametric monitoring system; data analysis; landslides; rock masses; slope stability

1. Introduction

Monitoring of slopes that are potentially involved in gravity-induced deformations has become a relevant topic in the last decades. The challenge is generally related to the transmission of alarm signals for early warning in the case of exposed infrastructures (such as railway, highways, pipelines and aqueducts) or natural and cultural heritage, as typically no significant deformations are detectable before failure occurrence. The recognition of failure precursors by multi-parametric monitoring systems, which is a sensor network able to monitor several kinds of parameters, in natural contexts as well as of the forcing actions that generate deformations is an important target in addressing this challenge. It is well known that changes in the stress conditions of rock masses due to impulsive or viscous deformations can cause rapid and violent failures able to widely affect slopes and generate landslides [1]. Furthermore, the ongoing deformational processes, which lead to failures of rock masses, represent a complex geomechanical topic because the jointing conditions, as well as the effective stress field, can strongly constrain precursors, such as microstrains or microcracks, which are also associated with acoustic or vibrational emissions [2–7].

Multi-parametric monitoring systems linked to early-warning procedures appear to be a very good solution for use in prevention plans and risk mitigation. Multi-parametric monitoring offers a temporary strategy to ensure public safety prior to implementing more definitive vulnerability reduction actions. Due to the recent developments in the computer science disciplines, monitoring system can benefit from the concept of cloud monitoring [8], which is devoted to early warning that requires huge data sets to be managed in very short time by (semi)automatic data flow-to-data processing analyses. The main peculiarities of cloud parametric monitoring systems (CPMS) are: (i) redundancy of the measurement data; (ii) secondary relevance of the a priori understanding of cause-to-effect relations of the monitored phenomena; (iii) reconstruction of the ex-post relations between destabilising causes and/or forcing factors and induced effects; and (iv) quantification of the alert levels and connected control index for infrastructure management. In this way, CPMS can be designed as part of a wireless sensors network (WSN) for real-time data transmission [9,10].

The setup of a multi-parametric monitoring system for an identified landslide hazard requires the identification of the most relevant factors with respect to the physical mechanisms, which potentially lead to slope failure to classify them into a hierarchy according to their role, impact, chronology and causality effects relative to the considered phenomenon [11]. Gunzburger et al. [12] divided these factors, which contribute to making a rock mass prone-to-failure, into three different categories: (i) *predisposition factors* are characteristic of the typology of the slope. Some slopes are, in fact, more susceptible than others to rock fall activity due to background factors, such as topography, vegetation, lithological parameters, and fracture geometry and density; (ii) *preparatory factors* are the cause of medium- to long-term changes in resistance. For monitoring to be efficient, their small and almost imperceptible effects must accumulate until rupture; (iii) *trigger factors* change over the short- to medium time frame and constitute the most direct causes of failure. Unlike *preparatory* and *trigger factors*, which are defined by their action period, *predisposition factors* do not exhibit any evolution over time. Detecting these factors before failure occurrence presents a challenge in multi-parametric system design [13]. Furthermore, these factors are strictly connected to the assessment and prediction of landslide hazards in the framework of a multi-parametric scenario. In this regard, the development of monitoring strategies devoted to take into account the numerous parameters which control the rock mass behaviour for assessing their influence on the slope stability provides a useful tool to mitigate geological risks [14,15].

Two methods have been widely used for natural hazard control and for managing the related risks. The first method, more focused on hazards, consists of monitoring the precursors of rock failures by a multi-parametric monitoring system mainly composed of seismic or micro-seismic devices, as well as acoustical emission [16–21]. The second method, equally focused on hazard and on vulnerability, consists on the observation of landslide source areas as well as of threatened infrastructures by using optical or interferometric devices for detecting fast morphological changes that are hazardous to the monitored infrastructures [22–26]. Several authors [27–29] have tried to combine these two strategies by using innovative devices, such as terrestrial laser scanners (TLS) and interferometric radar (GBInSAR), which are capable of inspecting an unstable slope with high spatial and temporal frequency, coupled with microseismic monitoring systems that provide deeper insight into the stress conditions within the rock mass. Multi-parametric monitoring systems devoted to risk mitigation involving strategic infrastructures (such as highways, railway and aqueducts) or workplaces (like mines and yards for underground excavation) are also of great relevance. Important examples can be found in mine work areas, where multi-parametric monitoring systems are installed with the aim of safe and reliable operations in the mining area [30,31]. To ensure post-mining risk management and public safety, several real-time microseismic monitoring systems and remote sensing networks have been installed to detect the ongoing jointing of rock masses as precursor events of an increasing strain rate that could anticipate slope collapse [32,33].

Where specific meteorological conditions exist, the surface temperature in outcropping rock masses fluctuates naturally under the influence of local weather conditions and can be sensitive to

thermal forcing related to cyclic expansion and contraction that can act over a long time, inducing cumulative deformations. These effects can influence the long-term behaviour of fractured rock masses, operating as a thermal fatigue process [34] and leading the joints of a rock mass to evolve towards failure [12,35–39]. Due to daily and seasonal temperature changes [40], rock failures can also occur when impulsive trigger factors (such as precipitation, seismic activity and freezing) are not effective. To address this issue, multi-parametric monitoring systems can be installed to evaluate the influence of thermo-mechanical effects [41–43] with particular attention to contexts where infrastructures are exposed to geological risk. Remote sensing techniques are, instead, suitable for recognizing the surficial temperature of rock masses through infrared thermography (IRT) applications [44–46]. Multi-parametric monitoring systems coupled with numerical modelling studies, focused on rock mass temperature and related rock strain, have also been applied for the preservation of relevant sites, also elected as natural heritage [47–49].

Several approaches have already been proposed in the literature for data analysis. The most widespread conventional approach is, undoubtedly, the deterministic approach (i.e., data-driven analysis), wherein relations among monitored data are physically based. The main fields of application of this approach include among others landslide susceptibility [50,51], microzonation studies [52], hydrogeology [53], and the study of rainfall-induced shallow landslides [54]. The stochastic model (in other words, the probabilistic one) is often opposed to the deterministic approach in the same field of application, especially in geological risk mitigation [55,56], as these types of models take into consideration all the possible variables that influence a given physical process. Considering instead time-dependent processes of very long duration, i.e., creep-driven deformations, the empirical method proposes to forecast the time of failure of complex geological phenomena [57–59]. The applications of statistical methods and, more in particular, of cross-correlation techniques are less common in the earth sciences field, which concern above all seismology or seismic and microseismic applications [60,61], palaeontology and ecology studies [62]. Several examples of test-sites worldwide are shown in literature, devoted to describing how several types of destabilising actions can lead rock masses to failure, analysing datasets using mainly data-driven approaches, also considering apparently unperturbed conditions [40,41,63,64].

Within the general framework just presented, the following of the paper shows the results of a comparison on the ability of three different approaches of data analysis to detect some mutual relations between destabilising factors and their related strain effects for implementing a multi-parametric data management through CPMS: an observation-based approach (OBA), a statistics (in cloud analysis)-based approach (SBA), and a semi-empirical approach (SEA). More in particular, the suitability of these approaches to provide specific relations as cause-to-effect link or statistical cross-correlations from environmental records (such as air temperature, rock temperature, rainfall, wind, induced vibration, and strains) was evaluated to better constrain the time windows suitable for driving rock mass deformations towards failure or general slope collapse. Even if these approaches are well known in literature and widely applied to analyse environmental datasets from monitoring systems they were never systematically compared, based on the authors' knowledge, by considering the same dataset in order to evaluate their suitability to detect deformative processes, involving rock masses at different time windows, since its start until the failure.

2. Multi-Parametric Monitoring of the Acuto Test-Site

To provide a dataset suitable to be analysed by the aforementioned approaches, a multi-parametric monitoring system was installed in an unstable quarry wall located close to the Acuto village in Central Italy, where densely jointed limestone is stressed under natural (temperature, rainfall and wind) and forced (induced vibrations) conditions.

The quarry is located in the western sector of the Simbruini-Ernici Mts. ridge where Mesozoic limestone outcrops [65]. The unstable rock wall extends almost 500 m in length and up to 50 m in height: it is SE-exposed and corresponds to the NW abutment of the quarry area.

Five main joint sets (S0 to S4) were recognized: S0 (93/4; dip direction/dip), S1 (131/82), S2 (91/64), S3 (4/80), S4 (198/86) that predispose the rock mass to failure with rock planar and wedge slide, rock fall and rock topple mechanisms with respect to the quarry wall attitude (100/88) [66,67]. The joint roughness coefficient (JRC) and the joint compressive strength (JCS) of the main joint sets were also estimated using a standard Barton profilometer and a Schmidt sclerometer, respectively [68] and the values of the intact rock friction angle (ϕ_b) were attributed based on the tilt test [69] (Table 1). The average uniaxial compression strength (UCS) of the rock was 130 MPa while the Young modulus of approximately 6×10^4 MPa, according to the Deere and Miller chart. The rock mass quality was established through RMRb classification, which assigned to the Mesozoic limestone a score of 68.

Table 1. Main geomechanical features of the joint sets recognized through remote and direct surveys.

Set	Dip Dir. (°)	Dip (°)	JCS (MPa)	JRC	ϕ (°)
0	93	4	180	3	53
1	131	82	120	8	54
2	91	64	130	3	49
3	4	80	110	4	49
4	198	86	140	5	50

A rock block of about 20 m^3 was selected as target of the multi-parametric monitoring system. The block is bounded by an open joint, which separates the backside from the rock mass behind, and hosts several fractures so providing a high number of discontinuities to be instrumented. Moreover, it protrudes with respect to the adjacent rock wall on the quarry square below.

The installed multi-parametric monitoring system consists of (see Figure 1): (i) a weather station (equipped with an air thermometer, hygrometer, rain gauge and anemometer for wind speed and direction) installed at the top of the slope; (ii) a rock thermometer (type-k thermocouple) to measure the rock mass temperature, installed at the centre of the monitored rock block; (iii) six HBM strain gages and foue extensometers, installed on micro-fractures and open-joints both on the frontal face of the block and on the backside face; and (iv) an optical cam (artificial intelligence camera prototype-AiCP) connected to a customized artificial intelligence (AI) system [24]. The recorded data, which are acquired each minute, are stored in a local CR1000 data logger (Campbell Scientific, Logan, UT 84321-1784, USA) and are automatically sent every 4 h to a local server through a GPRS antenna.

Figure 1. Monitored rock block (**a**) with both faces highlighted in the dashed boxes. Sensors installed on the rock block: (**b**) strain-gage, (**c**) type-k thermocouple to measure the rock mass temperature, (**d**) extensimeter, (**e**) weather station with a Campbell Scientific CR1000 data logger.

During specific experimental activities, the rock wall was stressed by dynamic actions to investigate its strain response. To this aim, the monitoring system was implemented through six on-rock mono-axial FBA11 accelerometers from KINEMETRICS (Pasadena, CA 91107, USA), three placed on the rock block and three on the rock wall, cable-connected to a KINEMETRICS K2 datalogger equipped with a tri-axial accelerometer placed at the slope foot and continuously acquired data a sampling rate of 250 Hz. The dynamic input was reproduced using a vibrodyne electro-mechanical excitation device, which is able to produce vibrations at a fixed frequency and amplitude in a range from 5 Hz to 25 Hz [70,71] (Figure 2). A vibrodyne was located on a concrete base at the foot of the instrumented rock block and was operated to induce frequencies in a range between 5 Hz and 25 Hz with an incremental step of 5 Hz. After each shaking sequence of variable duration to transmit the same amount of energy to the slope system, the experiment was interrupted for at least one hour with the aim to restore undisturbed vibrational conditions within the rock wall.

Figure 2. Devices installed at the Acuto test-site for the dynamic excitation experiments. The rock block is highlighted (**b**) with the disposition of the mono-axial accelerometers on the rock wall (black dashed circles) and on the rock block (red dashed circles). The mono-axial accelerometers installed on the ground (blue dashed circles) are shown in the main picture (**a**) with the vibrodyne device (**c**).

Table 2 summarises all the instrumental features of the devices composing the multisensor and multi-parametric monitoring system.

Table 2. Technical features of the installed devices.

Device	Measuring Range	Precision	Repeatability	Resolution	Linearity	Natural Frequency
Air Thermometer	−40/+60 °C	±0.1 K	±0.1 °C	-	-	-
Hygrometer	0–100% RH	±0.8% RH	>5% RH	-	-	-
Wind Speed	1.5/79 m/s	±1.5 m/s	-	0.1 m/s	-	-
Wind Direction	0–352°	±7°	-	-	-	-
Rain Gage (*standard WMO*)	-	±0.2 mm	-	0.2 mm H_2O	-	-
Rock Thermometer	−30/+100 °C	-	-	0.1 °C	±0.15 °C	-
Strain Gage (1-LY41-50/120)	50 mm (measurement base)	-	-	1 µstrain	-	-
Extensometer	25 mm (measurement base)	-	-	0.01 mm	0.5%	-
Accelerometer (KINEMETRICS FBA11)	±1 g	-	-	-	-	50 Hz

3. Approaches Compared for Multi-Parametric Data Analysis

Information about the evolution of a slope physical environment can be deduced carrying out a data analysis on multi-parametric monitoring system dataset. The design stage of the multi-sensors system architecture is based on a detailed engineering geological model, defined by direct-survey and remote-sensing techniques.

The data collected from the Acuto test-site were managed through the design of an appropriate cloud database and analysed following one of the three approaches described in the following part of this chapter (OBA, SBA, SEA), either one-by-one or by combining two or more together, to forecast the slope evolution. The goal is to evaluate the suitability of these compared approaches in establish relations between forcing actions and induced strain effects in different time windows, thus providing alert levels and fixing threshold values of the monitored parameters to improve the response time for interventions in the infrastructure management [72] (Figure 3).

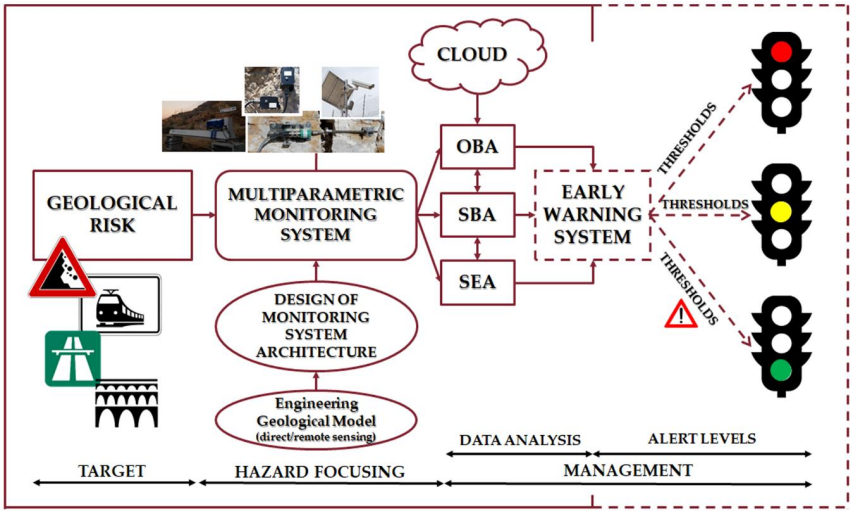

Figure 3. Flow chart showing the role of data management approaches in the frame of geological risk mitigation activities. The data from a multi-parametric monitoring system are processed through the proposed approaches for mitigation of the geological risk by a real-time early warning system. The continuous-line box indicates the themes and activities carried out in the frame of this research. The dashed-line box indicates the future calibration of an early warning system based on the results of the compared approaches (modified from Bozzano et al. [72]).

3.1. Observation-Based Approach

The OBA is based on searching for objective cause-to-effect relations among forcing actions and the induced strain effects. The OBA assumes that events are chained according to "cause-to-effect" logic relations based on a well-constrained geological-engineering and evolutionary model of the slope; therefore, site-specific knowledge is requested for the considered slope system.

Usually, continuous and discontinuous data are generally recorded by monitoring system. Continuous parameter recording represents a dataset that is monitored over time without null values but may be constant over a certain period, such as temperature. On the contrary, discontinuous parameter represents a dataset referring to transient or paroxysmal events related to impulsive actions featuring a certain intensity at a certain time, such as rainfall or wind. To search for objective cause-to-effect relations among the recorded datasets, the discontinuous data include the effects of triggers that are effective over an instant or short period, while the continuous data are related to longer and continuously forcing actions, the effects of which are visible over a medium-to-large time window. In this framework, OBA appears particularly suitable for investigating destabilising factors that induce a deformative response in the slope during a short- or medium to long- time window, with particular regard to impulsive destabilising factors.

3.2. Statistics-Based Approach

The SBA adopts, in our case, cross-correlation functions among different parameters and their rate variation to point out statistical relationships between two independent time series by testing the reciprocal dependence. More in particular, the cross-correlation measures the similarity of two series as a function of the time lag (LAG), which indicates the time delay between two signals and outputs a statistical coefficient (i.e., correlation function; CF) whose value increases at increasing coincidence between the time series.

The analysis presented herein was performed on the different time series using R open-source software [73], which returns a correlogram graph (i.e., CF vs. LAG). The LAG value indicates the time delay between two signals and is expressed as a multiple of the sampling step. After calculating the cross-correlation between the two signals, the maximum CF (a-dimensional) corresponds to the time at which the signals are best correlated. Two dotted lines are also depicted and represent the statistical significance threshold of the level of correlation (Figure 4).

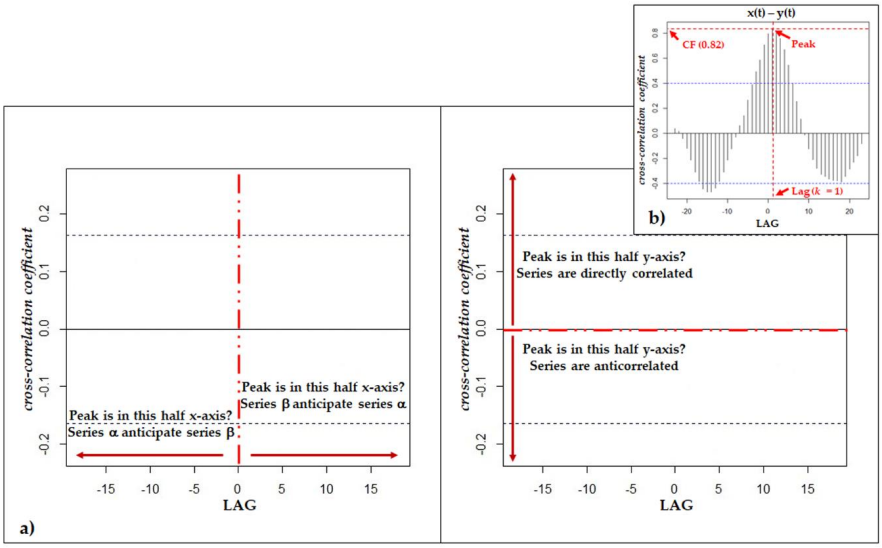

Figure 4. Sketch explaining how to read the correlogram and the interpretation of the peak (**a**) and an example of a correlogram obtained with R software (**b**). On the y-axis is shown the cross-correlation coefficient value and on the x-axis is shown the LAG value: y(t) anticipates the x(t) of a LAG time equal to 1 (that corresponds to the sampling step of the series) (**b**). The dashed lines indicate the values of statistical significance of the results.

The SBA was applied to the data series, expressed as the rate of monitored values: temperature, rainfall and wind with related strain series. The rate can: (i) increase, when transgressive processes can evolve towards a paroxysmal episodes; (ii) decrease, when regressive processes can reduce the failure occurrence taking into account a short and/or medium time window; (iii) remain constant, when stationary processes cannot evolve towards critical phases close in time, but could do it considering a long-time windows [74,75]. The rate of discontinuous data, as well as rainfall, can be analysed by accumulating them to derive typical ramp-and-flat variation curves. The ramps correspond to event occurrences; the flats indicate events did not occur. This analysis returns zero to non-null values in cases of occurrence or non-occurrence of triggering episodes. The rate of continuous data, as well as temperature, can be obtained by carrying out a linear regression analysis to detect a suite of events, as well as their variations over time.

In outputting possible response delays of the system with respect to different kinds of forcing actions, a correlation coefficient (R^2) can be attributed at each value of the rate, evaluating the effectiveness of a trend within a selected time window that must consist of at least 3 points. If the datasets are strongly scattered, the analysis return very low values of R^2, indicating an aleatory

variation of the considered variable. At the contrary, if the data are aligned the analysis return R^2 values up to 1, indicating a well-delineated trend of the considered variable. In our specific case, $R^2 \geq 0.75$ was considered as a reliable correlation coefficient value of both transgressive and regressive trend [76].

The rates of different datasets were here computed using a customised seismic analysis code (SAC) and FORTRAN UNIX scripts that firstly perform some pre-processing operations applied to each time histories of continuous (like as smoothing tool) and discontinuous (like as cumulative tool) monitored data. Successively, the linear regression, the R^2 factors and the rates of several time series within a specific time window were calculated (Figure 5). The time series of rates were cross correlated to determine which series influence the others and over what time range.

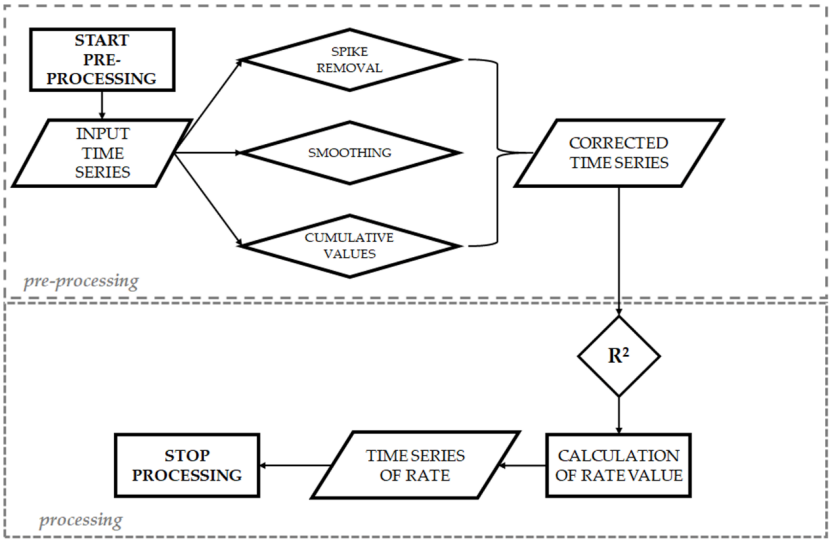

Figure 5. Flow chart illustrating the tools of the compiled script for rate analysis of the Acuto dataset, propaedeutic to cross-correlation statistical analysis of the obtained time series of rates.

3.3. Semi-Empirical Approach

The SEA is used to try to predict the time-to-failure of a physical system based on the hypothesis that such a failure represents the final stage of a creeping process, assuming simplified rheological models with their time-by-time calibration based on long-time monitoring time series. Such an approach does not necessarily need of a geologically based model of the slope, since it is not based on cause-to-effect relations. Moreover, it may allow for the temporal prediction of the slope failure, but it could fail for slope processes affected by relevant temporal changes of the controlling and triggering factors.

For slope stability applications, the SEA was originally experienced by Fukuzono [77] and based on results from laboratory tests that output relation between the velocity and the acceleration of displacement during the tertiary creep under stress and temperature constant conditions. Further semi-empirical methods known as material failure forecasting methods (FFMs) were developed to forecast the time-to-failure that induce hazardous events in a physical system [78]. Those methods are distinguished in: (i) graphical [77]; (ii) log rate vs. log acceleration [78]; (iii) linearized least square [76]; and (iv) non-linear least square [78]. These techniques take into account datasets from new monitoring technologies, such as SAR interferometry [79] and geotechnical devices [80], on which the inverse velocity model can be applied to forecast the time-to-failure of large-scale rock landslides [57].

To apply the SEA, a very long displacement dataset must be available to detect the transition to the tertiary creep phase as well as the definition of a rheological model of the physical slope system that is connected to a well-defined long-term mechanical response to external forces (e.g., deformation responses of the rock mass driven by viscous rheology or by thermomechanical processes). To define the most correct rheological models two approaches can be followed: (i) assuming a mechanical behaviour

based on the typology of the natural system and its composition; (ii) perform a machine learning through the recorded big-to-mega data from the monitoring system itself [81,82]. These models must be able to justify any long-term drifts in the rock mass deformation that can be interpreted as changes in the trend and, therefore, in the temporal evolution of a deformation process. In our case, we present preliminary results from only a 3 years of strain dataset, which, at most, can provide suggestions on the long-term evolution of the monitored process but not yet able to predict the failure time because the strain time series does not show deviations from their trend.

4. Results

The results obtained from the data recorded by the multi-parametric monitoring system installed at the Acuto test-site for comparing the three aforementioned approaches are presented in the following sections. The data acquisition was carried out starting from April 2016, and it was split in two phases: Phase A, in which weather and strain monitoring were carried out by continuous recording to detect daily and seasonal changes in rock behaviour due to natural forcing actions, and Phase B, carried out from 18th July to 21st July 2016, in which the rock block was forced by dynamic actions to induce strain effects under controlled conditions.

4.1. OBA Analysis

Weather conditions and induced strains were monitored by continuous data recording, detecting daily and seasonal changes due to temperature, rainfall and wind that can cause rock mass deformations. The air temperature, considered as the main possible continuous *preparatory factor* (*sensu* Gunzburger et al. [12]), showed daily and seasonal cyclic oscillations (Figure 6a) typical of the latitude and climatic zone in which the test-site is located. During the Summer season, the air temperature can exceed 30 °C, while in Winter, it may drop below 0 °C. The daily thermal excursion follows a similar trend to that of the average air temperature, showing the highest values (up to 16 °C) in the Spring and Summer seasons. The lower values (down to 2 °C) are concentrated in the Autumn and Winter, in conjunction with the decrease of the air temperature average values. The air temperature directly influences the rock temperature (Figure 6a), as its trend follows that of the air temperature very well. This occurs on both a daily and seasonal trend, revealing that the temperature is the main external forcing that continuously acts on the rock mass deformation (Figure 6a–blue line). Similarly to the trend of the air temperature, during the summertime, the rock temperature (Figure 6a) can exceed 40 °C thanks to the influence of direct solar radiation, while in wintertime, it may drop to −5 °C. The daily thermal excursion follows a more different trend relative to that of the average rock temperature. In fact, the highest values (up to 19 °C) were recorded in the Spring and Autumn seasons, and the lower values (down to 2 °C) were concentrated in the Summer and Winter seasons (Figure 6a–red line). The low Winter temperatures may give rise to freezing effects in the rock block, which are considered a *trigger factor* for micro-fracture propagation. The rock temperature, as well as the resulting deformation, is influenced not only by the air temperature but also primarily by the direct action of solar radiation, as shown by Fiorucci et al. [44]. In fact, the rock temperature value is greater than the air temperature value, also presenting the peak of the thermal maximum of each daily cycle generally anticipated with respect to that of the air temperature because of their different thermal conductivities. The role played by rainfall can be considered a *preparatory factor* in the case of regular occurrence or as a *trigger factor* in the case of intense and concentrated episodes. The rainfall regime (Figure 6b) also shows a seasonal trend, with frequent and intense rain concentrated in the Autumn and Spring months, during which the possibility of rock strain is highly. During the monitoring period, a total of 2034 mm of rain was cumulated, with a maximum daily precipitation of 82 mm/day that occurred in September 2017 (Figure 6b). Unlike the temperature that acts continuously and cyclically on the rock mass strain, the rainfall shows an aperiodic (or non-cyclical) behaviour. In addition, windstorms can be occasionally considered as a *trigger factor* for joint opening. Only events with the wind direction in an azimuth range between N 10° and N 190°, which is the same aspect

of the rock wall, can be taken into account. During the monitoring period, six strong windstorms occurred, characterised by wind speeds higher than the average value (15 m/s for each winter storm). In the considered case, a very small scatter in rock mass deformation trend occurred immediately after storm phenomena in the period during which rainfall was absent and the thermal input was constant, but, in principle, the wind does not seem to be a forcing able to make appreciable deformations in the natural system (Figure 6c). The values of strain sensors (both strain gages and extensometers) installed on the rock block show that a continuous deformational trend is ongoing both in micro fractures (monitored through strain gauges) and in open joints (monitored through extensometers). The sensor, which measured the highest displacement values both on daily time-window and in seasonal one, is the SG06 installed on the outer edge of the slope in very high release conditions. The rock mass strain is a direct expression of the cyclic temperature behaviour over both the daily and the seasonal time window. In fact, it shows the same 365/366 short-period daily and one long-period seasonal cycles characterised by large long-term oscillations (due to seasonal temperature fluctuations), which are overlapped with other smaller entities (due to daily thermal cycling; Figure 6d,e).

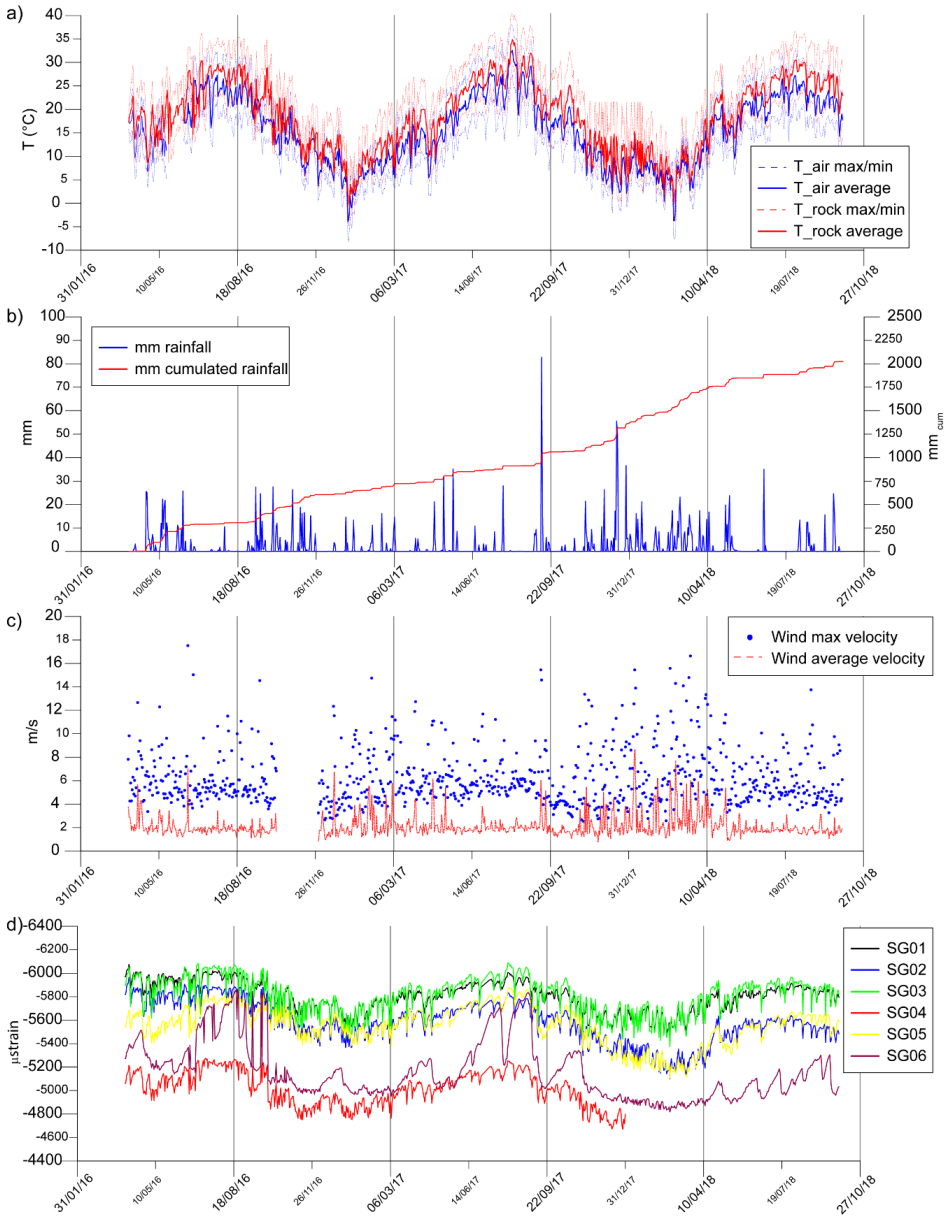

Figure 6. *Cont.*

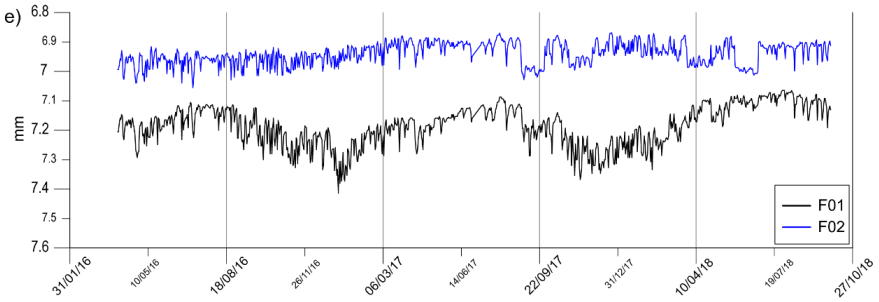

Figure 6. Data from the multi-parametric monitoring system: average daily values of the air temperature and rock temperature (**a**), daily rainfall and cumulated rainfall (**b**), average monthly wind speed with wind gusts (**c**), daily strain records from all strain gages (**d**) and from extensometers (**e**).

At the Acuto test-site, the daily thermal oscillation is considerable, especially during mid-seasons, therefore influencing the long-term behaviour of the rock mass [44,83], in addition to the daily deformation cycles that operate as a thermal fatigue process [34,84,85] and act as a continuous *preparatory factor* for rock failure and for displacement variation in open joints.

During each daily thermal cycle, a temperature heating phase is followed by a related cooling phase. The first phase, starting with sunrise until about midday, is due to direct solar radiation, and the second phase follows the first when the rock block progressively moves into shadow. The average monthly durations of the rock heating ramps are generally between approximately 5 and 7 h, while the average monthly durations of the air heating ramps are generally approximately 10 h. This time duration difference is due to the exposition to the East of the front face of the rock block, where the thermocouple is installed, which goes into shadow starting at 11:00 a.m. On the contrary, the average monthly durations of the air-cooling ramps are approximately 13 h, while the rock cools on average over a time window of approximately 18 h. The hour thermal rate, both for the air and for the rock, is greater for the heating ramp than for the cooling ramp. The maximum of the hour thermal rate values is reached during the Summer, while the minimum occurs during the Winter. The daily cyclic displacement reveals an almost thermo-elastic behaviour of the rock strain that represents the almost instantaneous response of the rock mass to the action of a continuous thermal stress. The values of the daily strain cycles are between 130 μstrain and 250 μstrain, depending on the considered season. As is the case for the temperature cycles, the amplitude of the strain cycles reach the maximum during the Summer season and the minimum during the Winter season. The heating ramp is always shorter than the related cooling ramp due to the effect of direct and strong solar radiation. In fact, the heating ramp presents an average monthly duration from 6 to 8 h, while the cooling ramp has an average monthly duration between 16 and 19 h. The average monthly strain rate related to the heating ramp presents higher values than those related to the cooling ramp, regardless of the month considered. The cooling phase is divided in two parts: the first occurs immediately after the rock goes into shadow, and the second occurs during the night. In the first part, the rock loses heat quickly, and the slope of the line is high. In the last daily part of the cooling phase, the rock loses heat more slowly, depending on the heat capacity value, and the slope of the line is lower than the previous slope (Figure 7).

By applying the OBA to induced forcing actions, it was possible to determine the dynamic behaviour of the rock block (assumed as the receiver site) with respect to the rock wall behind (assumed as the reference site). A standard spectral ratio (SSR) analysis [86] was carried out by taking into account the spectra obtained on the protruded rock block and on the rock wall behind, using the accelerometers above presented. This analysis points out an amplification in the block at 25 Hz in the cases of both 15 Hz and 20 Hz dynamic inputs. Moreover, time-to-frequencies analysis carried out on the recorded signals shows that at the lowest generated frequencies (5 and 10 Hz), no energy was received by the rock block, and, consequently, no significant induced vibration was detected. Instead, starting from the 15 Hz vibration, a very low response was detected for the rock block (Figure 8).

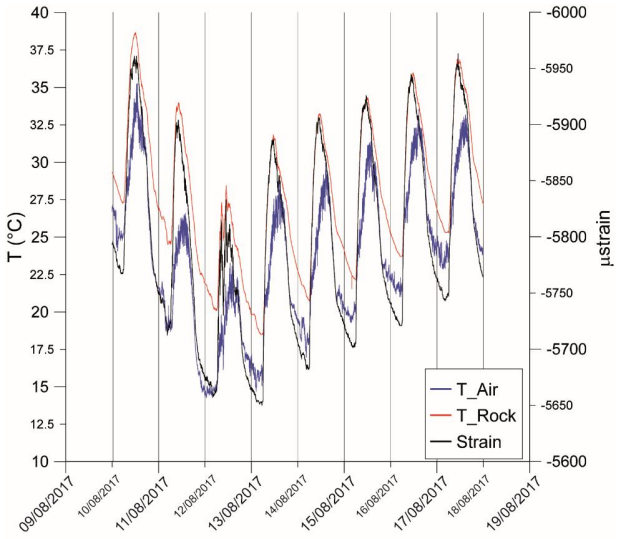

Figure 7. Example of the daily strain cycles over 10 days within the rock mass due to cyclic thermal input during the Summer season.

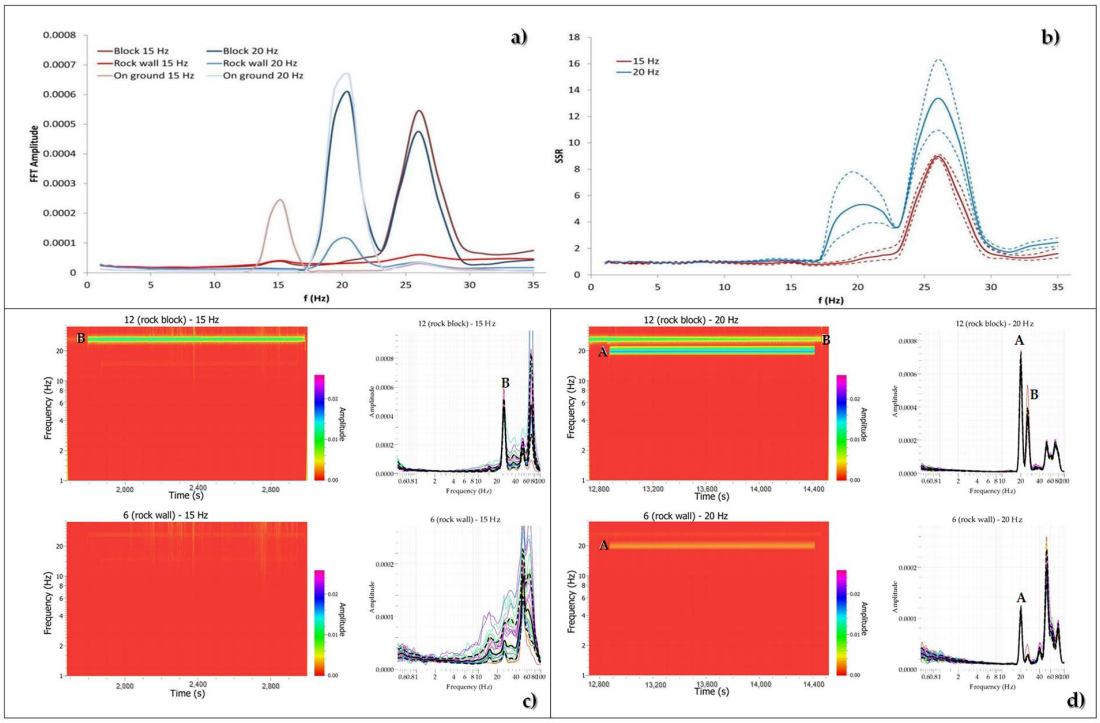

Figure 8. Fast Fourier transform, FFT (**a**), and block/wall SSR (**b**) obtained for the 15 Hz and 20 Hz shaking tests. The rock block dynamic amplification response at 20 Hz is visible (**b**). Dashed lines indicate the standard deviation values. Time-frequency analyses and spectral analyses obtained for the 15 Hz (**c**) and 20 Hz (**d**) shaking tests: on the rock block (up) and on the rock wall behind (bottom). Markers on the spectrograms indicate frequencies due to Vibrodyne excitation (A) and to the power unit supply (B). For the 20 Hz excitation, the possible dynamic response of the monitored rock block can be distinguished.

4.2. SBA Analysis

According to the SBA, the cross-correlation functions were defined between the time series of rate of the air temperature and the rock temperature, revealing very high correlation values. The time

series of rate of the air temperature always anticipates the time series of rate of the rock temperatures by approximately 10 min.

The cross-correlation function was also carried out to compare the time series of rate of the rock temperature and the time series of rate of the cumulative rainfall and wind speed to verify whether these last two forcing actions can influence the temperature of the rock block, thus changing the deformation response in the heating or cooling phases of daily or seasonal thermal cycles. The results of the statistical analysis show a slight influence of rainfall on the rock temperature, returning very low cross-correlation coefficient. No significant cross-correlation was found between the time series of rate of the wind speed and the time series of rate of the rock temperature (Figure 9).

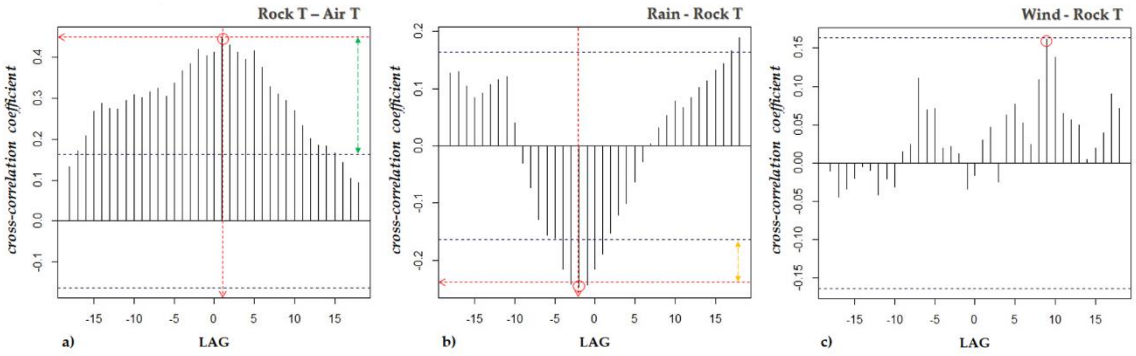

Figure 9. (**a**) Correlogram of the cross-correlation between the rock temperature and the air temperature. The air temperature always anticipates the rock temperature. The green arrow indicates the statistical significance of the result. (**b**) Correlogram of the cross-correlation between rainfall and the rock temperature. The rainfall anticipates the rock temperature, but with a very low CF value. The yellow arrow indicates the low statistical significance of the result. (**c**) Correlogram of the cross-correlation between the wind speed and the rock temperature. No peak of cross-correlation is evident on the graph, and the results remain below the statistical significance threshold. The LAG value is expressed as a multiple of the sampling step of R^2 (equal to 10 min, which represent the unit value of LAG).

The cross-correlation analyses were performed taking into account the time series of rate acquired over the entire monitoring period, during which several meteorological conditions (i.e., high or low rock temperatures, intense or absent rainfall, and strong wind speeds) were detected, representing potential destabilising actions for the stability of the monitored rock block. In accordance with the SBA, cross-correlations were carried out among the time series of rate of each considered forcing action, which were assumed as *preparatory factors* [12], and the time series of rate of the strain recorded along joints or micro-fractures. The obtained results show that rainfall and wind speed are always poorly or very poorly correlated with the rock mass strain. On the contrary, the rock temperature reveals a very good cross-correlation with the rock mass strain, demonstrating a significant influence on the rock mass deformation. In this case, no significant lag between the thermal action and the induced strain effect was observed, i.e., the high rock temperature can be regarded as the main forcing factor, which can cause a response of the jointed rock mass within a short to very short time.

The obtained results confirm that temperature pulsation is the most influencing factor for the strain effects induced in the outcropping rock mass. In this regard, all the strain devices return rate series that are always cross-correlated with the time series of rate of the rock temperature, and the CF value is always high and above the threshold of statistical significance, as it varies in a range from −0.3 in the Winter season, when the thermal input into the rock mass is low, to −0.8 in the Summer season, when the thermal input into the rock mass is higher (Figure 10).

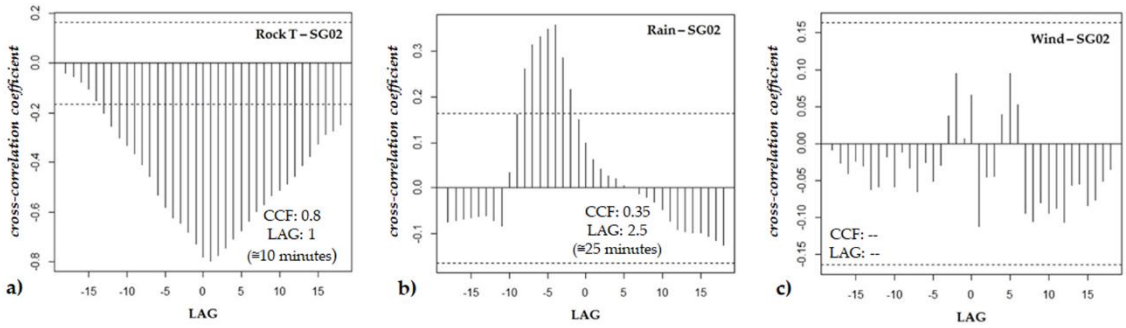

Figure 10. Correlograms indicating examples of cross-correlations between: (**a**) the rate series of the rock temperature and the strain; (**b**) the rate series of the rainfall and the strain; (**c**) the rate series of storm wind and the strain. The LAG value is expressed as a multiple of the sampling step of R^2 (equal to 10 min in our case).

4.3. SEA Analysis

During the total monitoring period (three years), the instrumented joints and micro-fractures did not show significant variation of the strain rates, which signifies that no changes of the rheological behaviour occurred that could lead the rock block to failure closely in time. However, the collected data demonstrated that cyclical temperature changes influence the strain rate measured in the rock mass, as they are responsible for the slight and regular accumulation of irreversible strain (plastic vs. elastic strain aliquots). In fact, part of the deformation due to thermal input occurs under elastic conditions, and it will be completely recovered at the end of the thermal cycle, while a very residual part of the deformation occurs under inelastic conditions; therefore, it will not be recovered at the end of the thermal cycle. For this reason, after each daily thermal cycle, the monitored rock mass could accumulates a slight net strain when two consecutive thermal cycles that have the same thermal excursion imply two consecutive strain cycles that present a very marked different amplitudes (i.e., the strain does not return to the starting value unlike the temperature). Such a net strain can be cumulated after a "critical" thermal cycle in the rock mass, in which the deformation cannot be recovered. The total cumulative strains recorded so far, due to inelastic effects, range from 55 up to 500 μstrain depending on the considered sensors (Figure 11).

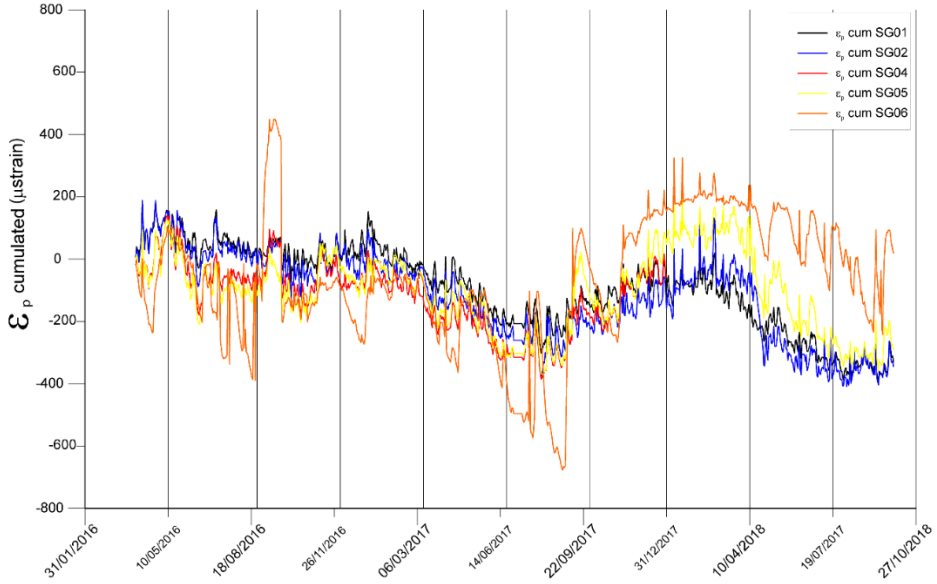

Figure 11. Net deformation value (ε_p), daily cumulated for each strain device.

Considering the cumulative value of net strains cumulated in the rock mass over a large (pluri-seasonal) time window, which are due to inelastic joint deformations, a steady creep-like behaviour results for the rock mass. Nevertheless, by decreasing the analysed time windows (i.e., tending to daily time window or, at most, pluri-diurnal), the observed time-dependent effect properly expresses a thermal fatigue phenomena, known as thermomechanical creep, acting on the monitored rock mass over long time windows; thermomechanical creep can lead towards failure conditions, as it could occur after accelerating creep. The preliminary SEA analysis, carried out in order to obtain the long period daily net deformation rate series on which will apply the FFMs methods, show that the maximum amplitude of this value and the higher frequency of peaks are concentrated in Spring and Autumn seasons. During these seasons, the following two main factors affected the amplitude of the net strain response: (i) the daily thermal excursion is higher than other seasons and (ii) the maximum and minimum thermal variations between two consecutive days is often not negligible.

5. Discussion

The three considered approaches to data analysis (OBA, SBA and SEA) have been compared here to evaluate their reliability for analysing and deducing relations among *preparatory factors* and the related strain effects, on micro-fractures and open joints of the outcropping rock mass, through different time windows (taking into account already well-known relations with the aim to testing these approaches with expected results). To this aim, each forcing action (i.e., temperature, rainfall, wind and induced vibrations) has been related to the induced rock mass strains using the three proposed approaches deriving inferences considering different time windows.

The OBA allows clearly deriving cause-to-effect relations due to continuous or impulsive forcing actions and related strain effects (Figure 12). The temperature shows a cyclical behaviour at different wavelengths over daily and seasonal time windows, whereas rainfall is characterised by cyclical recurrence over a seasonal time window only. The actions of these *preparatory factors* are reflected in a composed cyclic trend of the strain that, little by little, accumulates inelastic deformation (due to the daily net strain rate) over a longer time window (several seasons). For each daily thermal cycle, the OBA allowed outputting of the elastic contributions due to thermomechanical behaviour of the rock mass and defining and characterising the heating and cooling phases over daily and seasonal time windows.

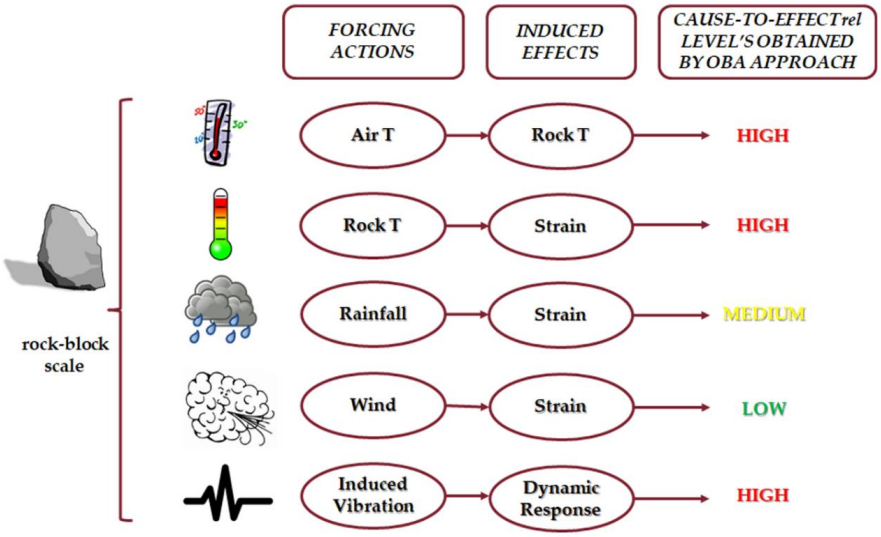

Figure 12. Results from the OBA experienced at the Acuto test-site with the associated severity levels from objective cause-to-effect relations.

Regarding the impulsive actions, objective cause-to-effect relations have also been deduced according to vibrations generated under controlled conditions (i.e., regularly emitted by engines), since the strain effects of the rock mass were evident in terms of the dynamic mobility and block resonance. On the contrary, impulsive but irregular forcing actions due to wind did not allow objective cause-to-effect relations with the strain effects measured in the rock mass, except for very intense events such as storms. By the OBA, the highest severity levels which could correspond to alert signals are related to the strongest and clearest cause-to-effect objective evidence, as in the cases of the air-to-rock temperature, rock temperature-to-strain, and man-induced vibrations-to-strain.

The SBA was carried out to define which rate series are cross correlated with each other over medium- to long time windows (i.e., daily tending towards seasonal). The main benefit of such a statistical approach is to automatically verify the occurrence of correlations among several data series, also allowing the estimation of the time lag over which two rate series are cross-correlated. All the data series of forcing actions have been cross correlated by considering the resulting rates of strain values to point out the redundancy of transgressive series, which can detect conditions leading towards failure. The results demonstrated that very high correlations exist between continuous and regular forcing actions and the induced strains, such as for rock temperature and thermomechanical effects over daily time windows, tending to seasonal. On the other hand, the data series are poorly cross correlated in the cases of irregular and discontinuous forcing actions, such as for rainfall or wind and the induced rock mass strain. The results show a high cross-correlation between the air temperature and the rock temperature, which implies a relevant correlation between the rock temperature rate and the strain rates, indicating the main role of heating and cooling cycles in destabilising the rock mass monitored at the Acuto test-site (Figure 13).

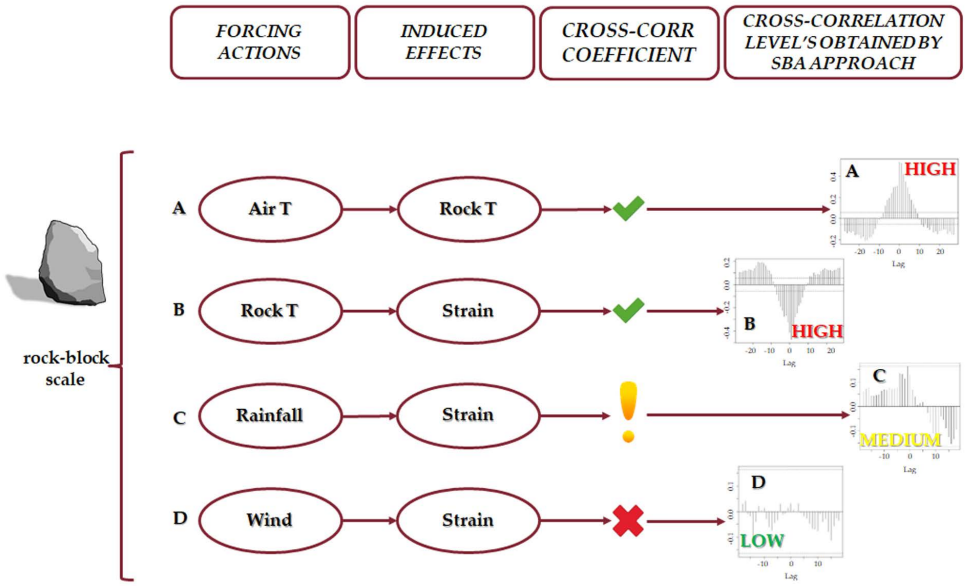

Figure 13. Results from the SBA experienced at the Acuto test-site with associated severity levels determined by cross-correlating causative forcing actions and the induced effects.

Based on the analysed dataset, the highest severity levels that could correspond to alert signals are also related to the strongest and clearest cross-correlation evidence in the case of the SBA, such as in the cases of the air-to-rock temperature, rock temperature-to-strain, and, secondly, man-induced vibrations-to-strain.

Therefore, the OBA and SBA output the same screening severity levels. Nevertheless, the advantage of the SBA with respect to the OBA is automatically providing the temporal lag, during which time a destabilising factor influences the deformational response of the rock mass. Thus, the OBA allows justification of the observed cause-to-effect relations in terms of a physical model of the monitored

system, i.e., by associating specific actions (such as temperature or vibrations) relative to the realistic elements (such as rock mass joints) that record the induced effect (i.e., strain).

The SEA was revealed to be more suitable for evaluating long-term behaviour, taking into account cumulative inelastic strain effects due to several destabilising actions (i.e., considered as the net resulting effect over time of *predisposing* and *preparatory factors*, *sensu* Gunzburger et al. [12]) which singularly act over specific time windows at the block-to-slope scale. In particular, at the Acuto test-site, the long-term behaviour mainly results as an effect of loading/unloading thermal cycles acting on the rock mass and the accumulating inelastic strains along joints as the sum of daily net deformations.

Based on the comparison analysis performed on dataset by the multi-parametric monitoring system at the Acuto test-site, the three considered approaches for multi-parametric data analysis can be regarded as more suitable and effective for different time windows, over which several forcing actions can induce objective rock mass strains. The OBA was more suitable for recognizing deformations induced over a shorter time window, i.e., those due to continuous or cyclical forcing actions, as well as impulsive and dynamic input (i.e., hourly to seasonal and instantaneous). The SBA was more suitable for recognizing continuous or cumulative trend variations responsible for strains over time, highlighted by differences in the cross-correlation coefficient or by a lack of it taking into account the same forcing actions, of the deformation response over medium- to long time windows (i.e., daily tending towards seasonal). The SEA was more suitable for detecting deformational trends over very long time windows (i.e., plurennial), i.e., those due to the cumulative effects of different forcing actions characterised by cyclical or continuous occurrence (Figure 14).

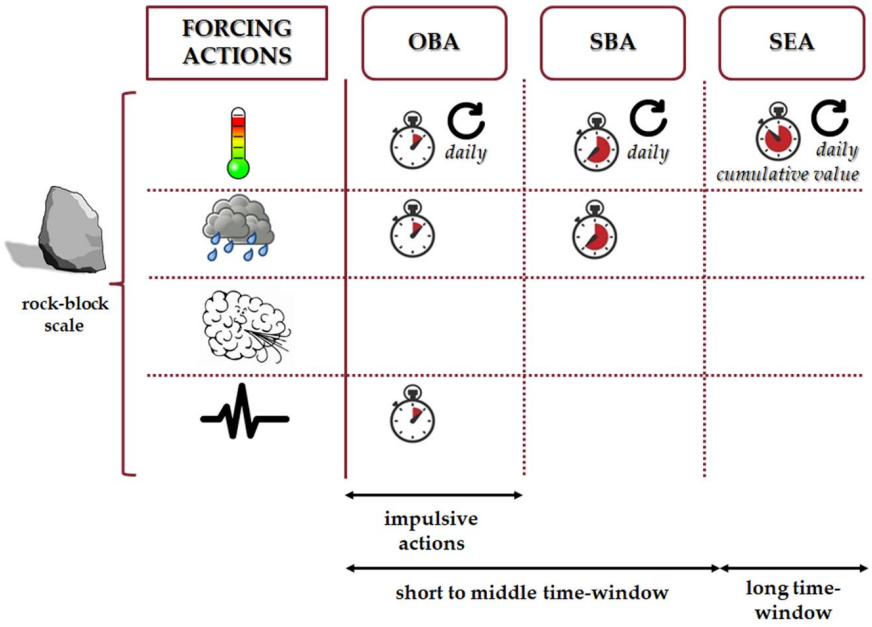

Figure 14. Summary table showing the applicability of the proposed approaches for detecting factors influencing the rock mass stability at the Acuto test-site. The clocks indicate the time windows (i.e., from short- to long-term) over which specific factors are effective. The loop arrows indicate that the considered processes are cyclical.

By considering a long-time window, the cumulative effects of several continuous, cyclic or transient forcing actions can generate a deformative response of the rock mass that leads the physical system, whether a natural or anthropogenic rock slope, towards failure conditions. These strain effects can occur in a rock mass both through the simultaneous action of several forcing actions and through the continuous action over the time of the same forcing. The existent relations among the forcing actions and the directly related deformative responses can be investigated by applying a specific data analysis approach from those presented above. For each considered forcing action, the efficiency of each

approach was evaluated in terms of its ability to detect the related strain effects. In particular, the strain due to the cyclic action of temperature daily fluctuations in the rock was detected by all presented approaches, thus confirming the severity of thermal input in affecting rock mass deformation. On the contrary, all approaches verified that there were no deformations in the rock mass due to the action of the wind, confirming its scarce ability to induce rock mass deformations. Considering the rainfall forcing, only one approach detected a possible rock deformation because of this action. In this case, the non-occurrence of the redundancy of the same result by the application of the three approaches confirms the lesser role of rainfall in rock mass deformations. In other words, if a single forcing action contributing to induce rock mass deformations is detected by several approaches, the severity of the considered cause-to-effect relation will be greater, and vice versa (Figure 15).

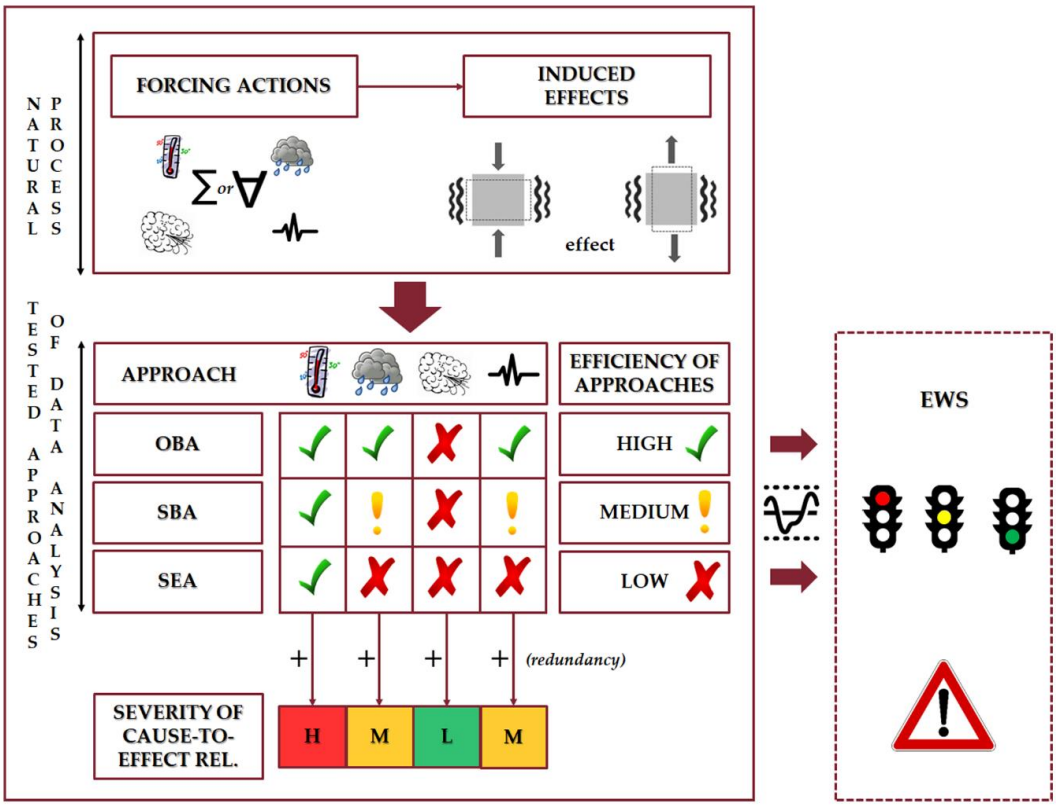

Figure 15. Flow chart illustrating the suitability of the compared approaches for data analysis based on the data recorded by the multi-parametric monitoring system installed at the Acuto test-site with the aim of mitigating the geological risk related to several destabilising actions which induce strain effects on the monitored rock-mass. The continuous-line box indicates the themes and activities carried out in the frame of this research. The dashed-line box indicates the future calibration of an early warning system based on the results of the compared approaches.

6. Conclusions

To provide a more reliable risk mitigation strategy, three commonly applied data analysis approaches were compared in this study to evaluate their suitability for detecting well-known causative co-relations among forcing actions and induced effects over different time window. The OBA was revealed to be more suitable for the detection of cyclical and impulsive events, i.e., those with regular and continuous recurrence over a shorter time window. The SBA was appeared to be more suitable for detecting transgressive series of causing factors and the induced effects, which are cross correlated over a medium to long time window so returning the lag time of influence. The SEA was demonstrated to be powerful for detecting the strain rate variation due to rheological behaviours over long- to very long-time windows.

In particular, for the considered case study of the Acuto test-site (i.e., considering the time of occurrence of destabilising factors here monitored), the temperature was demonstrated to be the main preparatory factor (*sensu* Gunzburger et al. [12]) in rock mass deformation due to its daily and seasonal oscillation (results obtained mainly by the OBA), which triggered a deformation response of the monitored joints and micro-fractures over a period of 10 min when the daily thermal cycle was considered (results obtained mainly by the SBA). Considering a very long-time window, the daily thermal input involves net strains accumulated in the rock mass due to thermal fatigue phenomena that can lead the rock block towards failure conditions (results obtained by the SEA). Seasonal cycles accumulating over several months, i.e., over a long-time window, result in an inelastic strain which causes a creep-like trend over a multi-season time window. On the contrary, impulsive destabilising actions, such as intense rainfall and windstorms, did not regularly induce strain effects that were objectively linked to causative actions. The results here presented were obtained by considering the size of the Acuto rock block, but the efficiency of the considered approaches can be transposed both to smaller and larger sizing (i.e., by rock sample to rock wall or rock slope size).

The approaches discussed herein will be efficiently combined to provide a warning strategy for landslide risk mitigation by stressing their redundancy to: (i) identify precursor signals, so minimising the time for interventions, analysing cause-to-effect relations between forcing actions and strains over short to medium time windows; (ii) compute, through the cross-correlation function, time lags between forcing actions and the resulting strain effects over medium to long time windows; and (iii) detect long-term irreversible strain effects over long- to very long time windows.

Author Contributions: M.F. and S.M. conceptualised and designed the multi-parametric monitoring system. M.F. performed the field experiments and collected and analysed the monitoring data here presented as results. S.M., F.B., and A.P. supervised and coordinated the research activities. All authors contributed to the interpretation and the discussion of the results and wrote the manuscript. All authors have read and agreed to the published version of the manuscript.

Funding: This research received no external funding.

Acknowledgments: The research was carried out in the framework of a Ph.D. project "Approaches of data analysis from multi-parametric monitoring systems for landslide risk management", conducted by Ph.D. Matteo Fiorucci with tutor Salvatore Martino. The Authors wish to thank the two external reviews of the Ph.D. thesis, Matteo Berti and Veronique Merrien-Soukatchoff, for their useful remarks, and Antonella Paciello (ENEA National Agency) for her support in the data processing. The research is framed in the MIUR "Departments of Excellence" 2018–2022 project, of which the Acuto quarry is one of the selected test-site. Moreover, since August 2018 the quarry was entrusted on free loan for research aims by the Acuto Municipality to the CERI Research Centre of the "Sapienza" University of Rome.

Conflicts of Interest: The authors declare that there are no conflict of interest regarding the publication of this paper.

References

1. Evans, S.; Mugnozza, G.S.; Strom, A. *Landslides from Massive Rock Slope Failure*; Nato Science Series; Series IV: Earth Environ Sci; Springer: Dordrecht, The Netherlands, 2006; Volume 49, p. 662.
2. Bottelin, P.; Jongmans, D.; Daudon, D.; Mathy, A.; Helmstetter, A.; Bonilla-Sierra, V.; Cadet, H.; Amitrano, D.; Richefeu, V.; Lorier, L.; et al. Seismic and mechanical studies of the artificially triggered rockfall at Mount Néron (French Alps, December 2011). *Nat. Hazards Earth Syst. Sci.* **2014**, *14*, 3175–3193. [CrossRef]
3. Lévy, C.; Baillet, L.; Jongmans, D.; Mourot, P.; Hantz, D. Dynamic response of the Chamousset rock column (Western Alps, France). *J. Geophys. Res.* **2010**, *115*, F04043. [CrossRef]
4. Lévy, C.; Jongmans, D.; Baillet, L. Analysis of seismic signals recorded on a prone-to-fall rock column (Vercors massif, French Alps). *Geophys. J. Int.* **2011**, *186*, 296–310. [CrossRef]
5. Mercerat, E.D.; Driad-Lebeau, L.; Bernard, P. Induced Seismicity Monitoring of an Underground Salt Cavern Prone to Collapse. *Pure Appl. Geophys.* **2010**, *167*, 5–25. [CrossRef]
6. Senfaute, G.; Duperret, A.; Lawrence, J.A. Micro-seismic precursory cracks prior to rock-fall on coastal chalk cliffs: A case study at Mesnil-Val, Normandie, NW France. *Nat. Hazards Earth Syst. Sci.* **2009**, *9*, 1625–1641. [CrossRef]

7. Walter, M.; Schwaderer, U.; Joswig, M. Seismic monitoring of precursory fracture signals from a destructive rockfall in the Vorarlberg Alps, Austria. *Nat. Hazards Earth Syst. Sci.* **2012**, *12*, 3545–3555. [CrossRef]
8. Bigarré, P.; Verdel, T.; Klein, E.; Gueniffey, Y. Cloud monitoring: An innovative approach for the prevention of landslide risks. In Proceedings of the Second World Landslide Forum, Rome, Italy, 3–7 October 2011; pp. 1–5.
9. Fantini, A.; Magrini, M.; Martino, S.; Moroni, D.; Pieri, G.; Prestininzi, A.; Salvetti, O. Experiencing embedded sensors network for the early warning management of natural risks due to fast-failures along railways. In Proceedings of the 5th International Workshop on Image Mining. Theory and Applications, Berlin, Germany, 11–14 March 2015; pp. 85–91.
10. Rosi, A.; Berti, M.; Bicocchi, N.; Castelli, G.; Corsini, A.; Mamei, M.; Zambonelli, F. Landslide monitoring with sensor networks: Experiences and lessons learnt from a real-world deployment. *Int. J. Sens. Netw.* **2011**, *10*, 111. [CrossRef]
11. Klein, E.; Nadim, C.; Bigarré, P.; Dünner, C. Global monitoring strategy applied to ground failure hazards. In Proceedings of the 10th International Symposium on Landslides and Engineered, Xi'an, China, 30 June–4 July 2008; pp. 1925–1931.
12. Gunzburger, Y.; Merrien-Soukatchoff, V.; Guglielmi, Y. Influence of daily surface temperature fluctuations on rock slope stability: Case study of the Rochers de Valabres slope (France). *Int. J. Rock Mech. Min. Sci.* **2005**, *42*, 331–349. [CrossRef]
13. Kilburn, C.R.J.; Petley, D.N. Forecasting giant, catastrophic slope collapse: Lessons from Vajont, Northern Italy. *Geomorphology* **2003**, *54*, 21–32. [CrossRef]
14. KhaloKakaie, R.; Zare Naghadehi, M. The assessment of rock slope instability along the Khosh-Yeylagh Main Road (Iran) using a systems approach. *Environ. Earth Sci.* **2012**, *67*, 665–682. [CrossRef]
15. Rozos, D.; Pyrgiotis, L.; Skias, S.; Tsagaratos, P. An implementation of rock engineering system for ranking the instability potential of natural slopes in Greek territory. An application in Karditsa County. *Landslides* **2008**, *5*, 261–270. [CrossRef]
16. Amitrano, D.; Grasso, J.R.; Senfaute, G. Seismic precursory patterns before a cliff collapse and critical point phenomena. *Geophys. Res. Lett.* **2005**, *32*, L08314. [CrossRef]
17. Amitrano, D.; Arattano, M.; Chiarle, M.; Mortara, G.; Occhiena, C.; Pirulli, M.; Scavia, C. Microseismic activity analysis for the study of the rupture mechanisms in unstable rock masses. *Nat. Hazards Earth Syst. Sci.* **2010**, *10*, 831–841. [CrossRef]
18. Arosio, D.; Longoni, L.; Papini, M.; Boccolari, M.; Zanzi, L. Analysis of microseismic signals collected on an unstable rock face in the Italian Prealps. *Geophys. J. Int.* **2018**, *213*, 475–488. [CrossRef]
19. Gaffet, S.; Guglielmi, Y.; Cappa, F.; Pambrun, C.; Monfret, T.; Amitrano, D. Use of the simultaneous seismic, GPS and meteorological monitoring for the characterization of a large unstable mountain slope in the southern French Alps. *Geophys. J. Int.* **2010**, *182*, 1395–1410. [CrossRef]
20. Xu, N.W.; Tang, C.A.; Li, L.C.; Zhou, Z.; Sha, C.; Liang, Z.Z.; Jang, J.Y. Microseismic monitoring and stability analysis of the left bank slope in Jinping first stage hydropower station in southwestern China. *Int. J. Rock Mech. Min. Sci.* **2011**, *48*, 950–963. [CrossRef]
21. Xu, N.W.; Li, T.B.; Dai, F.; Li, B.; Zhu, Y.G.; Yang, D.S. Microseismic monitoring and stability evaluation for the large scale underground caverns at the Houziyan hydropower station in Southwest China. *Eng. Geol.* **2015**, *188*, 48–67. [CrossRef]
22. Antonello, G.; Casagli, N.; Farina, P.; Leva, D.; Nico, G.; Sieber, A.J.; Tarchi, D. Ground-based SAR interferometry for monitoring mass movements. *Landslides* **2004**, *1*, 21–28. [CrossRef]
23. Barla, G.; Antolini, F.; Barla, M.; Mensi, E.; Piovano, G. Monitoring of the Beauregard landslide (Aosta Valley, Italy) using advanced and conventional techniques. *Eng. Geol.* **2010**, *116*, 218–235. [CrossRef]
24. Fantini, A.; Fiorucci, M.; Martino, S. Rock Falls Impacting Railway Tracks: Detection Analysis through an Artificial Intelligence Camera Prototype. *Wirel. Commun. Mob. Com.* **2017**, 9386928. [CrossRef]
25. Martino, S.; Mazzanti, P. Integrating geomechanical surveys and remote sensing for sea cliff slope stability analysis: The Mt. Pucci case study (Italy). *Nat. Hazards Earth Syst. Sci.* **2014**, *14*, 831–848. [CrossRef]
26. Niethammer, U.; James, M.R.; Rothmund, S.; Travelletti, J.; Joswig, M. UAV-based remote sensing of the Super-Sauze landslide: Evaluation and results. *Eng. Geol.* **2012**, *128*, 2–11. [CrossRef]

27. Arosio, D.; Longoni, L.; Papini, M.; Scaioni, M.; Zanzi, L.; Alba, M. Towards rockfall forecasting through observing deformations and listening to microseismic emissions. *Nat. Hazards Earth Syst. Sci.* **2009**, *9*, 1119–1131. [CrossRef]
28. Gigli, G.; Fanti, R.; Canuti, P.; Casagli, N. Integration of advanced monitoring and numerical modeling techniques for the complete risk scenario analysis of rockslides: The case of Mt. Beni (Florence, Italy). *Eng. Geol.* **2011**, *120*, 48–59. [CrossRef]
29. Janeras, M.; Jara, J.A.; Lopez, F.; Marturia, J.; Royan, M.J.; Vilaplana, J.M.; Aguasca, A.; Fabregas, X.; Cabranes, F.; Gili, J.A. Using several monitoring techniques to measure the rock mass deformation in the Montserrat Massif. *IOP Conf. Ser. Earth Environ. Sci.* **2015**, *26*, 01230. [CrossRef]
30. Cai, M.; Kaiser, P.K.; Martin, C.D. Quantification of rock mass damage in underground excavations from microseismic event monitoring. *Int. J. Rock Mech. Min. Sci.* **2001**, *38*, 1135–1145. [CrossRef]
31. Lai, X.P.; Cai, M.F.; Xie, M.W. In situ monitoring and analysis of rock mass behavior prior to collapse of the main transport roadway in Linglong Gold Mine, China. *Int. J. Rock Mech. Min. Sci.* **2006**, *43*, 640–646. [CrossRef]
32. Contrucci, I.; Klein, E.; Bigarré, P.; Lizeur, A.; Lomax, A.; Bennani, M. Management of post-mining large-scale ground failures: Blast swarms field experiment for calibration of permanent microseismic early-warning systems. *Pure Appl. Geophys.* **2010**, *167*, 43–62. [CrossRef]
33. Contrucci, I.; Klein, E.; Cao, N.-T.; Daupley, X.; Bigarré, P. Multi-parameter monitoring of a solution mining cavern collapse: First insight of precursors. *Comptes Rendus Geosci.* **2011**, *343*, 1–10. [CrossRef]
34. Hall, K. The role of thermal stress fatigue in the breakdown of rock in cold regions. *Geomorphology* **1999**, *31*, 47–63. [CrossRef]
35. Gischig, V.S.; Moore, J.R.; Evans, K.F.; Amann, F.; Loew, S. Thermomechanical forcing of deep rock slope deformation: 1. Conceptual study of a simplified slope. *J. Geophys. Res. Earth Surf.* **2011**, *116*, 1–18. [CrossRef]
36. Gischig, V.S.; Moore, J.R.; Evans, K.F.; Amann, F.; Loew, S. Thermomechanical forcing of deep rock slope deformation: 2. The Randa rock slope instability. *J. Geophys. Res. Earth Surf.* **2011**, *116*, 1–17. [CrossRef]
37. Grøneng, G.; Christiansen, H.H.; Nilsen, B.; Blikra, L.H. Meteorological effects on seasonal displacements of the Åknes rockslide, western Norway. *Landslides* **2011**, *8*, 1–15. [CrossRef]
38. Gunzburger, Y.; Merrien-Soukatchoff, V. Near-surface temperatures and heat balance of bare outcrops exposed to solar radiation. *Earth Surf. Process. Landf.* **2011**, *36*, 1577–1589. [CrossRef]
39. Pasten, C.; García, M.; Cortes, D.D. Physical and numerical modelling of the thermally induced wedging mechanism. *Geotech. Lett.* **2015**, *5*, 186–190. [CrossRef]
40. Collins, B.D.; Stock, G.M. Rockfall triggering by cyclic thermal stressing of exfoliation fractures. *Nat. Geosci.* **2016**, 2686. [CrossRef]
41. Bakun-Mazor, D.; Hatzor, Y.H.; Glaser, S.D. Carlos Santamarina, J. Thermally vs. seismically induced block displacements in Masada rock slopes. *Int. J. Rock Mech. Min. Sci.* **2013**, *61*, 196–211. [CrossRef]
42. Hatzor, Y.H. Keyblock Stability in Seismically Active Rock Slopes—Snake Path Cliff, Masada. *J. Geotech. Geoenviron. Eng.* **2003**, *129*, 697–710. [CrossRef]
43. Taboada, A.; Ginouvez, H.; Renouf, M.; Azemard, P. Landsliding generated by thermomechanical interactions between rock columns and wedging blocks: Study case from the Larzac Plateau (Southern France). *EPJ Web Conf.* **2017**, *140*, 14012. [CrossRef]
44. Fiorucci, M.; Marmoni, G.M.; Martino, S.; Mazzanti, P. Thermal Response of Jointed Rock Masses Inferred from Infrared Thermographic Surveying (Acuto Test-Site, Italy). *Sensors* **2018**, *18*, 2221. [CrossRef]
45. Frodella, W.; Gigli, G.; Morelli, S.; Lombardi, L.; Casagli, N. Landslide Mapping and Characterization through Infrared Thermography (IRT): Suggestions for a Methodological Approach from Some Case Studies. *Remote Sens.* **2017**, *9*, 1281. [CrossRef]
46. Pappalardo, G.; Mineo, S.; Perriello Zampelli, S.; Cubito, A.; Calcaterra, D. InfreRed Thermography proposed for the estimation of the Cooling Rate Index in the remote survey of rock masses. *Int. J. Rock Mech. Min. Sci.* **2016**, *83*, 182–196. [CrossRef]
47. Greif, V.; Brcek, M.; Vlcko, J.; Varilova, Z.; Zvelebil, J. Thermomechanical behavior of Pravcicka Brana Rock Arch (Czech Republic). *Landslides* **2017**, *14*, 1441–1455. [CrossRef]
48. Marmoni, G.M.; Fiorucci, M.; Grechi, G.; Martino, S. Modelling of thermo-mechanical effects in a rock quarry wall induced by near-surface temperature fluctuations. *Int. J. Rock Mech. Min. Sci.* **2020**, *134*, 104440. [CrossRef]

49. Vlcko, J.; Brcek, M.; Greif, V. Deformations Dynamics in Response to Seasonal Temperature Oscillations: An Example from Pravcicka Brana Rock Arch (Czech Republic). *Landslide Sci. Safer Geoenviron.* **2014**, *3*, 363–368.
50. Frattini, P.; Crosta, G.B.; Carrara, A.; Agliardi, F. Assessment of rockfall susceptibility by integrating statistical and physically-based approaches. *Geomorphology* **2008**, *94*, 419–437. [CrossRef]
51. Cervi, F.; Berti, M.; Borgatti, L.; Ronchetti, F.; Manenti, F.; Corsini, A. Comparing predictive capability of statistical and deterministic methods for landslide susceptibility mapping: A case study in the northern Apennines (Reggio Emilia Province, Italy). *Landslides* **2010**, *7*, 433–444. [CrossRef]
52. Pergalani, F.; Pagliaroli, A.; Bourdeau, C.; Compagnoni, M.; Lenti, L.; Lualdi, M.; Madiai, C.; Martino, S.; Razzano, R.; Varone, C.; et al. Seismic microzoning map: Approaches, results and applications after the 2016–2017 Central Italy seismic sequence. *Bull. Earthq. Eng.* **2020**, *18*, 5595–5629. [CrossRef]
53. Curtis, Z.K.; Li, S.G.; Liao, H.S.; Lusch, D. Data-driven approach for analyzing hydrogeology and groundwater quality across multiple scales. *Groundwater* **2018**, *56*, 377–398. [CrossRef]
54. Schilirò, L.; Montrasio, L.; Scarascia Mugnozza, G. Prediction of shallow landslide occurrence: Validation of a physically-based approach through a real case study. *Sci. Total Environ.* **2016**, *569*, 134–144. [CrossRef]
55. Stead, D.; Eberhardt, E.; Coggan, J.S. Developments in the characterization of complex rock slope deformation and failure using numerical modelling techniques. *Eng. Geol.* **2006**, *83*, 217–235. [CrossRef]
56. Martino, S.; Battaglia, S.; D'Alessandro, F.; Della Seta, M.; Esposito, C.; Martini, G.; Pallone, F.; Troiani, F. Earthquake-induced landslide scenarios for seismic microzonation: Application to the Accumoli area (Rieti, Italy). *Bull. Earthq. Eng.* **2020**, *18*, 5655–5673. [CrossRef]
57. Crosta, G.B.; Agliardi, F. Failure forecast for large rock slides by surface displacement measurements. *Can. Geotech. J.* **2003**, *40*, 176–191. [CrossRef]
58. Dick, G.J.; Eberhardt, E.; Cabrejo-Liévano, A.G.; Stead, D.; Rose, N.D. Development of an early-warning time-of-failure analysis methodology for open-pit mine slopes utilizing ground-based slope stability radar monitoring data. *Can. Geotech. J.* **2014**, *52*, 515–529. [CrossRef]
59. Mazzanti, P.; Bozzano, F.; Cipriani, I.; Prestininzi, A. New insights into the temporal prediction of landslides by a terrestrial SAR interferometry monitoring case study. *Landslides* **2015**, *12*, 55–68. [CrossRef]
60. Helmstetter, A.; Garambois, S. Seismic monitoring of Séchilienne rockslide (French Alps): Analysis of seismic signals and their correlation with rainfalls. *J. Geophys. Res. Earth Surf.* **2010**, *115*, 1–15. [CrossRef]
61. Del Gaudio, V.; Muscillo, S.; Wasowski, J. What we can learn about slope response to earthquakes from ambient noise analysis: An overview. *Eng. Geol.* **2014**, *182*, 182–200. [CrossRef]
62. Liow, L.H.; Reitan, T.; Harnik, P.G. Ecological interactions on macroevolutionary time scales: Clams and brachiopods are more than ships that pass in the night. *Ecol. Lett.* **2015**, *18*, 1030–1039. [CrossRef]
63. Andersson, P.; Wass, E. Aspo Hard Rock Laboratory. Aspo pillar stability experiment. Final Report, Rock mass response to coupled mechanical thermal loading. *SKBTR* **1999**.
64. Alcaíno-Olivares, R.; Perras, M.A.; Ziegler, M.; Maissen, J. Cliff stability at tomb KV42 in the Valley of the Kings, Egypt: A first approach to numerical modelling and site investigation. In Proceedings of the 53rd U.S. Rock Mechanics/Geomechanics Symposium, New York, NY, USA, 23–26 June 2019.
65. Accordi, G.; Carbone, F.; Civitelli, G.; Corda, L.; De Rita, D.; Esu, D.; Funiciello, R.; Kotsakis, T.; Mariotti, G.; Sposato, A. Lithofacies map of Latium- Abruzzi and neighbouring areas. *Quaderno C.N.R. La Ricerca Scientifica* **1986**, *114*, 1–223.
66. Fantini, A.; Fiorucci, M.; Martino, S.; Paciello, A. Investigating Rock Mass Failure Precursors Using a Multi-Sensor Monitoring System: Preliminary Results from a Test-Site (Acuto, Italy). *Procedia Eng.* **2017**, *191*, 188–195. [CrossRef]
67. Fantini, A.; Fiorucci, M.; Martino, S.; Sarandrea, P. 3D Remote survey of a rock wall hosting a multi-sensor monitoring system in a test-site (Acuto, Italy). *Rend. Online Soc. Geol. It.* **2017**, *42*, 30–33. [CrossRef]
68. ISRM. The Complete ISRM Suggested Methods for Rock Characterization, Testing and Monitoring: 1974–2006. In *ISRM & ISRM Turkish National Group*; Ulusay, R., Hudson, J.A., Eds.; ISRM Commissions on Testing Methods: Ankara, Turkey, 2007; p. 628, ISBN 978-975-93675-4-1.
69. Hoek, E.; Bray, J. *Rock Slope Engineering*; CRC Press: London, UK, 1981.
70. D'Angiò, D.; Curi, L.; Fiorucci, M.; Iannucci, R.; Lenti, L.; Martino, S.; Paciello, A. Fractured rock mass response to induced vibrations: Preliminary results from two test sites. In Proceedings of the 36° Convegno Nazionale del Gruppo Nazionale di Geofisica della Terra Solida (GNGTS), Trieste, Italy, 14–16 November 2017; pp. 696–700.

71. D'Angiò, D.; Fiorucci, M.; Lenti, L.; Martino, S.; Paciello, A. Preliminary results of vibration modes induced by forced dynamic shaking in a quarry rock wall. In Proceedings of the Progressive Rock Failure Conference, Monte Verità, Switzerland, 5–9 June 2017, Paper n° 04F-16.
72. Bozzano, F.; Esposito, C.; Fantini, A.; Fiorucci, M.; Martino, S.; Mazzanti, P.; Prestininzi, P.; Rivellino, S.; Rocca, A.; Scarascia Mugnozza, G. Multisensor Landslide Monitoring as a Challenge for Early Warning: From Process Based to Statistic Based Approaches. In *Advancing Culture of Living with Landslides*; Mikoš, M., Vilímek, V., Yin, Y., Sassa, K., Eds.; Springer: Cham, Switzerland, 2017; Volume 3, pp. 33–39.
73. R Core Team. *R: A Language and Environment for Statistical Computing*; R Foundation for Statistical Computing: Vienna, Austria, 2015; Available online: http://www.R-project.org/ (accessed on 1 August 2020).
74. Szwedzicki, T. Geotechnical precursors to large-scale ground collapse in mines. *Int. J. Rock Mech. Min. Sci.* **2001**, *38*, 957–965. [CrossRef]
75. Szwedzicki, T. Rock mass behaviour prior to failure. *Int. J. Rock Mech. Min. Sci.* **2003**, *40*, 573–584. [CrossRef]
76. Lenti, L.; Martino, S.; Paciello, A.; Prestininzi, A.; Rivellino, S. Microseismicity within a karstified rock mass due to cracks and collapses as a tool for risk management. *Nat. Hazards* **2012**, *64*, 359–379. [CrossRef]
77. Fukuzono, T. A new method for predicting the failure time of a slope. In Proceedings of the 4th International Conference and Field Workshop on Landslides, Tokyo, Japan, 23–31 August 1985; pp. 145–150.
78. Cornelius, R.R.; Voight, B. Graphical and PC-software analysis of volcano eruption precursors according to the Materials Failure Forecast Method (FFM). *J. Volcanol. Geotherm. Res.* **1995**, *64*, 295–320. [CrossRef]
79. Moretto, S.; Bozzano, F.; Esposito, C.; Mazzanti, P.; Rocca, A. Assessment of Landslide Pre-Failure Monitoring and Forecasting Using Satellite SAR Interferometry. *Geosciences* **2017**, *7*, 36. [CrossRef]
80. Segalini, A.; Valletta, A.; Carri, A. Landslide time-of-failure forecast and alert threshold assessment: A generalized criterion. *Eng. Geol.* **2018**, *245*, 72–80. [CrossRef]
81. Cherkassky, V.; Krasnopolsky, V.; Solomatine, D.P.; Valdes, J. Computational intelligence in earth sciences and environmental applications: Issues and challenges. *Neural Netw.* **2006**, *19*, 113–121. [CrossRef]
82. Toms, B.A.; Barnes, E.A.; Ebert-Uphoff, I. Physically interpretable neural networks for the geosciences: Applications to earth system variability. *J. Adv. Model.* **2020**, *12*, e2019MS002002.
83. Fiorucci, M.; Marmoni, G.M.; Martino, S.; Paciello, A. Experimental evidences of thermo-mechanical induced effects on jointed rock masses through infrared thermography and stress-strain monitoring. In *Geomechanics and Geodynamics of Rock Masses*; Litvinenko, V., Ed.; Taylor & Francis Group: London, UK, 2018; Volume 1, pp. 263–268.
84. Attewell, P.B.; Farmer, I.W. Fatigue behaviour of rock. *Int. J. Rock Mech. Min. Sci.* **1973**, *10*, 1–9. [CrossRef]
85. Cerfontaine, B.; Collin, F. Cyclic and Fatigue Behaviour of Rock Materials: Review, Interpretation and Research Perspectives. *Rock. Mech. Rock. Eng.* **2018**, *51*, 391–414. [CrossRef]
86. Borcherdt, R.D. Effects of local geology on ground motion near San Francisco Bay. *Bull. Seismol. Soc. Am.* **1970**, *60*, 29–61.

Publisher's Note: MDPI stays neutral with regard to jurisdictional claims in published maps and institutional affiliations.

© 2020 by the authors. Licensee MDPI, Basel, Switzerland. This article is an open access article distributed under the terms and conditions of the Creative Commons Attribution (CC BY) license (http://creativecommons.org/licenses/by/4.0/).